Dynamics of Nematic Liquid Crystal Disclinations: The Role of the Backflow

C. Blanc,[1] D. Svenšek,[2,3] S. Žumer,[2] and M. Nobili[1]

[1]*Laboratoire des colloïdes, verres et nanomatériaux, UMR 5587, CNRS-Université Montpellier II, Place E. Bataillon, 34095 Montpellier, France*

[2]*Department of Physics, University of Ljubljana, Jadranska 19, SI-1000 Ljubljana, Slovenia*

[3]*Theoretische Physik III, Universität Bayreuth, D-95440 Bayreuth, Germany*

(Received 9 March 2005; published 23 August 2005)

We measure the electric-field-driven annihilation of nematic disclination pairs with strength $\pm 1/2$ in the 4-cyano-4′-*n*-pentylbiphenyl (5CB) liquid crystal. The use of a very weak azimuthal anchoring ensures a two-dimensional director field. The relaxation is governed by the formation of a π wall connecting the two opposite charge defects. The $+1/2$ disclinations move almost twice as fast as the $-1/2$ disclinations. The simple used geometry allows a quantitative comparison with numerical studies based on the hydrodynamics of the tensorial order parameter. The simulations show that in the π wall regime the symmetry breaking is due to the backflow and not to the elastic anisotropy.

DOI: 10.1103/PhysRevLett.95.097802 PACS numbers: 61.30.Jf, 61.30.Hn, 61.72.Cc

The dynamics of topological defects plays an essential role in many areas of physics from cosmic strings in the early universe [1] to vortex lines in superfluid helium [2]. In many condensed matter systems, topological defects propagate in an almost motionless background as flux line dynamics in superconductors [3] and dislocation motion in crystals [4]. On the contrary, in softer systems such as nematic liquid crystals, a coupling between the propagation of topological defects and the flow field is expected. The topological defects (disclinations) [5] of a nematic liquid crystal are the singularities of the orientational field or *director* **n**, classified according to their topological charge (the winding number of the director field around the defect). When a defect moves, the surrounding elastic field changes and, accordingly, the director reorients. This director rotation is coupled with the velocity field by the so-called backflow effect. The backflow influence on the annihilation dynamics of $+1/2$ and $-1/2$ line defects has been addressed only recently by numerical simulations [6–8], according to which defects of opposite strength annihilate with different velocities. This surprising symmetry breaking is either induced by a different coupling with the flow field [7,8] or by the elastic anisotropy [7]. However, to the best of our knowledge a direct and clear experimental evidence of this symmetry breaking dynamics is still lacking.

In this Letter, we present an experimental study of the dynamics of $+1/2$ and $-1/2$ disclinations under the influence of an electric field. By using an original anchoring, we succeed in obtaining a two-dimensional (2D) director field. This simple experimental geometry allows an easy comparison with a 2D numerical simulation of the complete hydrodynamic equations [9,10]. We observe that the $+1/2$ line defect can move almost twice as fast as the $-1/2$ one in a wide range of applied forces. This velocity asymmetry is recovered in the simulations to a remarkable level of agreement, showing for the first time that complete simulations of disclination dynamics agree quantitatively with experiments.

We have used planar orienting layers with an almost memory-free anchoring for the 4-cyano-4′-*n*-pentylbiphenyl (5CB) nematic liquid crystal, providing a strong zenithal anchoring [11] but only a very weak azimuthal anchoring, thus enabling a free rotation of the director in the plane of the substrates. Two surface treatments have been examined: the memory-free standard (3-glycidoxypropyl) trimethoxysilane (3-GPS) [12] and a commercial photopolymer (Norland Optical Adhesive 60: NOA60). Here we discuss results obtained with NOA60, which gives a better temporal stability of the anchoring than 3-GPS. A solution (1 wt. % of NOA60 in ethanol) is spin coated on clean glass slides. After curing for 1 h in an oven at 90 °C, the slides are exposed to UV light for 10 minutes. Two parallel aluminum stripes $D \sim 1$ mm apart are then used both as spacers to mount the cells and as electrodes to apply a 10 kHz ac voltage V_a. The range of studied cell thickness d is 25–100 μm. In this geometry, the in-plane electric field is nearly constant at the mid-distance of electrodes with $E \approx 0.7V_a/D$ [13]. The cells are filled with 5CB and placed in an Instec STC200D oven, at fixed temperature $T_{\mathrm{eq}} = 32.3$ °C (the nematic-isotropic transition temperature is $T_{\mathrm{NI}} = 35.3$ °C). The region between electrodes is observed under a polarizing microscope equipped with a fast CCD camera (Pulnix TM-6703) and a PC frame grabber with the ability of capturing up to 100 frames/s.

We handle the weak residual azimuthal anchoring by applying a large electric field ($E > 100$ V/mm) for several hours before experiments. It fixes the easy axis in the direction perpendicular to the electrodes. The azimuthal anchoring is very weak with an extrapolation length as large as $L_{\mathrm{az}} \sim 100$ μm; see below. Disclinations are created in the electric field by moving a hot wire close to the cell, so that the temperature locally increases above T_{NI}.

After withdrawal, the sudden return to T_{eq} provokes the nucleation of wedge $\pm 1/2$ disclinations in the otherwise aligned sample. In the electric field, these defects annihilate by pairs of opposite topological charge.

An example of such an isolated pair is given in Fig. 1. A π wall connects the two vertical defects, corresponding to a π rotation of the director as shown by the presence of the two bright fringes observed under crossed polarizers. When increasing the electric field, the width of the π wall is observed to decrease strongly (Fig. 2) while the disclinations move much faster.

We first focus on the static π wall far from the moving disclinations, where no flow is present. Both the equilibrium texture and the energy stored in the wall result from the competition between elasticity, dielectric energy, and surface anchoring. One should distinguish two regimes depending on the electric field strength. In zero field, only the weak azimuthal surface anchoring competes with the bulk elasticity. The analytical expression of the director field is given in Ref. [14]. From a quantitative analysis of the transmitted intensity across the wall, we found a large surface extrapolation length L_{az} in the range 70–100 μm at T_{eq}. In a strong enough electric field, the anchoring becomes negligible and the free energy reduces to a bulk free energy:

$$F_b = \frac{1}{2}K(\nabla\varphi)^2 - \frac{1}{2}\varepsilon_0\varepsilon_a E^2\cos^2\varphi, \qquad (1)$$

where K is the splay-bend elastic modulus in the one-constant approximation, φ is the angle between the director and the electric field, and ε_a the dielectric anisotropy. For a π wall, minimization of Eq. (1) yields $\varphi(s) = 2\arctan[\exp(-s/\xi_E)]$, where $\xi_E = (K/\varepsilon_0\varepsilon_a)^{1/2}E^{-1}$ is the electric coherence length and s is a coordinate perpendicular to the π wall.

For an accurate measurement of the π wall width l, we set crossed polarizers with the analyzer parallel to the electric field. The transmitted intensity was then fitted with $I(s) \propto \cos^2[\varphi(s)]\sin^2[\varphi(s)]$ where we use $\varphi(s) = 2\arctan[\exp(-s/l)]$. Figure 2 shows the evolution of l with the applied voltage V_a. We find a linear relation $l = \beta V_a^{-1}$ for voltage larger than $V_c \approx 20$ V with $\beta \approx 300$ μm V. This shows that the above 2D director field correctly describes the texture above V_c (using the 5CB material parameters at T_{eq}, $K = 4 \times 10^{-12}$ N [15,16], $\varepsilon_a = 9.5$ [17], we obtain $\xi_E = \beta_{th}V_a^{-1}$ with $\beta_{th} = 312$ μm V). Accordingly, we neglect the surface anchoring in this regime.

We focus now on the stationary dynamics of a single defect reached under the external field. Note that this regime is not observed in the case of the free defect pair without the external field where defects accelerate [7,8]. Each disclination is subject to the same driving force equal to the π wall energy per unit length F. Under this force, disclinations acquire stationary velocities; this regime is observed as long as the distance between defects is larger than l. For distances lower than l, the disclinations accelerate. This behavior is due to the appearing of a supplementary force induced by the direct elastic interaction between the disclinations. Similar regimes (stationary and then accelerated at short separation distances) were also observed in presence of a strong anchoring alone [14]. In the following we will focus only on the stationary regime. Figure 3 shows the velocity dependence of each defect on the electric field for the case when the π wall is oriented at $\theta = 90°$ with respect to the field. Experimental points are obtained by averaging approximately 20 runs for each defect strength.

The $+1/2$ defect moves nearly twice as fast as the $-1/2$ one. Above E_c (corresponding to V_c), the defect velocities $v_\pm$ depend linearly on the electric field: $v_\pm = \alpha_\pm(E - e_p)$, where $\alpha_\pm$ are the mobility coefficients for each defect. This can be qualitatively understood by a competition of the driving force $F = 2Ed\sqrt{K\varepsilon_a\varepsilon_0}$ obtained from Eq. (1), a viscous drag force $\propto v_\pm$, and a weak constant force corresponding to the term e_p. The latter represents a friction force due to the interaction between the defects and the substrates. To overcome it, E should be larger than the

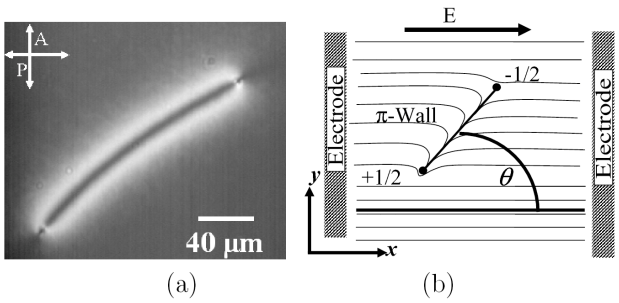

FIG. 1. (a) A pair of $\pm 1/2$ wedge disclinations connected by a π wall when an in-plane electric field is present ($E = 28$ V/mm). The disclinations remain vertical due to the strong zenithal anchoring. Thickness of the sample $d = 25$ μm, crossed polarizers. (b) Sketch of the 2D director field; θ is the angle between the π wall and the electric field.

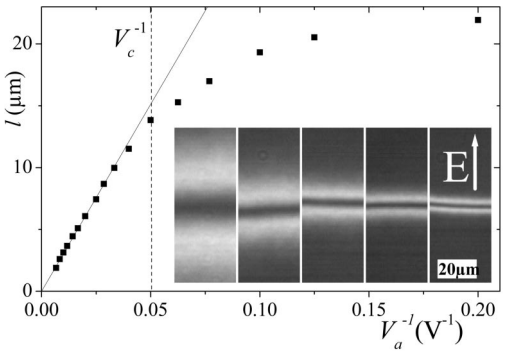

FIG. 2. The π wall width l strongly decreases with the applied voltage V_a. For large enough voltages, a linear relation is obtained, $l = \beta V_a^{-1}$, with $\beta \approx 298$ μm V. The insert shows some corresponding textures (from left to right $V_a = 0$, 30, 50, 70, 120 V); $d = 25$ μm, $D = 1$ mm, crossed polarizers.

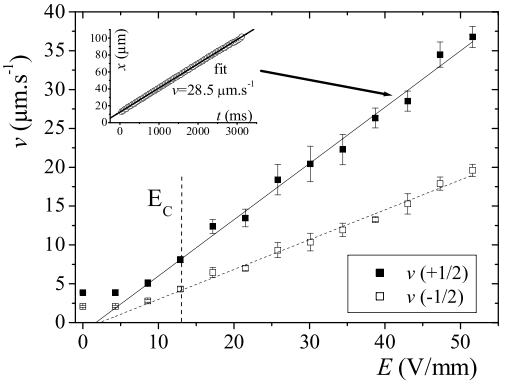

FIG. 3. Velocities of the $+1/2$ and $-1/2$ defects in a pair as a function of the local electric field E; $\theta = 90°$; $d = 25\ \mu$m. Inset: distance vs time for a $+1/2$ defect at an electric field of 43 V/mm.

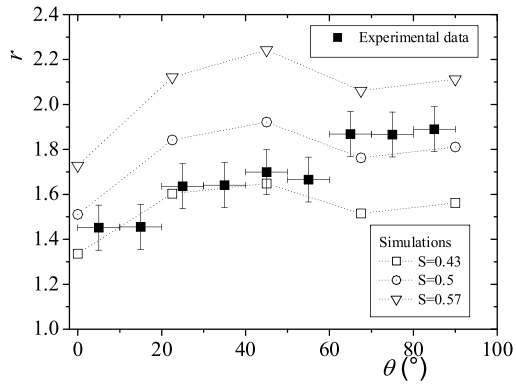

FIG. 4. Black squares: ratio $r = v_+/v_-$ vs angle θ between the π wall and the electric field; $E = 35$ V/mm, $d = 25\ \mu$m. Empty marks: simulated r for three different degrees of nematic order. $S \approx 0.5$ is expected at T_{eq}.

threshold field e_p [18]. We quantify the symmetry breaking by the ratio $r = \alpha_+/\alpha_-$. In Fig. 3, the linear fits (straight lines) are obtained with $\alpha_+ = 724\ \mu\mathrm{m}^2/(\mathrm{V\,s})$ and $\alpha_- = 384\ \mu\mathrm{m}^2/(\mathrm{V\,s})$, which yields $r = 1.89$. Similar measurements have been done in different samples, for different thicknesses and in a small temperature range ($T_{\mathrm{eq}} \pm 2\,°\mathrm{C}$). The ratio r is found constant ($r = 1.9 \pm 0.1$) even if some scattering of α_+ and α_- is observed [$\alpha_+ = 830 \pm 110\ \mu\mathrm{m}^2/(\mathrm{V\,s})$ and $\alpha_- = 440 \pm 60\ \mu\mathrm{m}^2/(\mathrm{V\,s})$ [19]]. Similar results are found with the 3-GPS surface treatment. We do not observe a clear influence of the cell thickness, as expected for a 2D system. The ratio r depends on the angle θ (Fig. 4): it increases with θ and reaches a maximum when the π wall is orthogonal to the electric field ($\theta = 90°$).

A simple analysis by neglecting the flow allows us to estimate $\alpha_\pm$ as a function of the 5CB parameters. We consider a π wall located at $y < 0$ in the defect frame. For a stationary dynamics, the drag force is $F_d = d\gamma_1 v_\pm \iint(\partial\varphi/\partial y)^2 dxdy$, where γ_1 is the rotational viscosity. In the quasistatic approximation, φ is given by $\nabla^2\varphi = \sin(2\varphi)/(2\xi_E^2)$ [from Eq. (1)] [20]. Note that in dimensionless cylindrical coordinates centered on the defect ($\tilde{r} = r/\xi_E, \phi$), φ does not depend on ξ_E. To compute the drag force F_d, we introduce a fixed adimensioned length $\tilde{r}_f$ which checks $a/\xi_E < \tilde{r}_f \ll 1$ where $a \sim 5$ nm is the elastic cutoff radius. We then compute F_d integral separately in the cylinder of radius $\tilde{r}_f$ and in the outer region. In the cylinder the influence of the electric field can be neglected and the director field is given by $\varphi \approx \pm(\phi/2 - \pi/4)$. Straightforward computations yield:

$$F_d \approx \frac{\pi}{4} d\gamma_1 v_\pm \ln\left(b\frac{\xi_E}{a}\right), \tag{2}$$

where $b = \tilde{r}_f \exp[(4/\pi)\int_{\tilde{r}_f}^{\infty}\int_0^{2\pi}(\partial\varphi/\partial\tilde{y})^2\tilde{r}d\tilde{r}d\phi]$ does not depend on ξ_E. Numerical computations of b give $b \approx 0.9 \pm 0.05$ for the range $0.05 < \tilde{r}_f < 0.1$. Balancing the driving force by this viscous force yields:

$$\alpha_\pm = \frac{8\sqrt{K\varepsilon_a\varepsilon_0}}{\pi\gamma_1 \ln(b\frac{\xi_E}{a})}. \tag{3}$$

Taking $\gamma_1 = 0.034$ Pa s [21], $\xi_E = 5\ \mu$m, and $a \sim 5$ nm, we obtain $\alpha_\pm \approx 200\ \mu\mathrm{m}^2/(\mathrm{V\,s})$, which is of the same magnitude as the measured values.

Such an analysis, however, neglects the backflow and the anisotropy of elastic constants and fails to reproduce the measured symmetry breaking dynamics. To account for it, a 2D hydrodynamic simulation based on the Q tensor description was performed. The governing equations, which comprise the dynamic equation for the Q tensor, the Navier-Stokes equation in the low-Reynolds-number and steady-state approximations, and the incompressibility requirement are explained in [8], together with the numerical technique. Here we extend the description to take into account the elastic anisotropy, which is realized by including in distortion energy density terms up to third order in Q:

$$f_d = \frac{1}{2}L(\partial_i \mathsf{Q}_{jk})^2 + \frac{1}{2}L'(\partial_i \mathsf{Q}_{ik})(\partial_j \mathsf{Q}_{jk}) + \frac{1}{2}L''\mathsf{Q}_{ij}(\partial_i \mathsf{Q}_{kl})(\partial_j \mathsf{Q}_{kl}), \tag{4}$$

where $L = (K_{33} + 2K_{22} - K_{11})/(9S^2)$, $L' = 4(K_{11} - K_{22})/(9S^2)$, and $L'' = 2(K_{33} - K_{11})/(9S^3)$ are expressed in terms of the Frank elastic constants K_{ii} and degree of order S. The Q-dependent part of the dielectric energy density is $f_E = -\frac{1}{3}\varepsilon_0\varepsilon_{\mathrm{am}}\mathsf{Q}_{ij}E_iE_j$, where $\varepsilon_{\mathrm{am}}$ is the microscopic electric anisotropy ($\varepsilon_a = S\varepsilon_{\mathrm{am}}$). Data on elastic constants and degree of order are taken from Refs. [15,16], Leslie viscosities from Ref. [5], and the coefficients describing the N-I transition from Ref. [22].

We simulate isolated $\pm 1/2$ defects on a $250a \times 250a$ grid. The electric field is chosen so that the π wall width is as narrow as $l \approx 75a$, while $l \gg a$ is still adequately satisfied. The simulated π wall width is much smaller than the experimental ones. This shortens the time scale; combining Eq. (3) and $E \propto \xi_E^{-1} \approx l^{-1}$, the defect velocity

scales as $v \propto [l \ln(l/a)]^{-1}$ and time scales as $t \propto l^2 \ln(l/a)$. The Navier-Stokes equation is linear in the velocity [8] and the viscous stress tensor σ^v which is the source of the symmetry breaking scales as $\sigma^v \propto [l^2 \ln(l/a)]^{-1}$. This means that the flow velocity scales in the same way as the defect velocity. The simulated system is thus just a downscale version of the actual one and the symmetry breaking is the same. The scaling is not perfect due to the elastic stress tensor σ^e [8] which scales as $\sigma^e \propto l^{-2}$, so that its influence in the downscale version is smaller in relative.

We start the simulation with the one-constant equilibrium configuration of the $\pm 1/2$ disclination, fix its core, and wait until the structure relaxes in the electric field forming the π wall. We let the defect propagate first without the flow to acquire a dynamic configuration. Then we run the simulation with the flow until the defect velocity is saturated. The velocity of the $+1/2$ defect is now typically twice as large, whereas the $-1/2$ defect is accelerated only weakly. We find that the elastic anisotropy does not contribute to the symmetry breaking. This can be understood as the π wall is energetically identical for both defects and so is thus the driving force. Only the inner director field around the defect at radii smaller than ξ_E differs elastically for the defect and antidefect, but it does not contribute to the driving force as it stays the same during the motion. On the contrary, in the absence of an external field [7,23], the whole director field is changing and the elastic anisotropy does contribute appreciably.

We have added in Fig. 4 the simulated values of r for a set of θ orientations and for three different values of the degree of order S (we expect $S \approx 0.5$ at T_{eq} [16]). They agree well with the measured ones and the θ dependence is partly recovered. Furthermore, one can roughly compensate for the different scaling of σ^e by using typical magnitudes of the flow generated separately by σ^v and σ^e and taking into account $\ln(l_{\mathrm{expt}}/a)/\ln(l_{\mathrm{sim}}/a) \approx 2$, as well as the empirical fact that σ^e does not contribute to the asymmetry. Such an estimate shifts the simulated points for the size of the error bar towards lower r values. The simulations show that the symmetry breaking is sensitive to the value of S. The extreme values of S given in Fig. 4, however, correspond to a rather large temperature range (~ 12 K). The ratio r is thus only slightly sensitive to the temperature (close to T_{eq}) in agreement with our experimental findings.

To conclude, we have presented the first experimental study of the dynamics of half-integer nematic disclinations with opposite charges in an external field. In 5CB, the $+1/2$ disclinations move systematically faster than the $-1/2$ ones. The chosen quasi-2D experimental geometry with field-screened interaction between the defect and antidefect allows a direct comparison with 2D numerical simulations. The main features of the dynamics have been retrieved, showing that in the π wall regime the asymmetry comes entirely from the backflow.

This work was partially supported by Slovenian Office of Science (P1-0099) and AvH Foundation.

[1] N. Turok, Phys. Rev. Lett. **63**, 2625 (1989).
[2] D. V. Osborne, Proc. Phys. Soc. London, Sect. A **63**, 909 (1950).
[3] G. Blatter *et al.*, Rev. Mod. Phys. **66**, 1125 (1994).
[4] F. R. N. Nabarro, *Theory of Dislocations* (Oxford University Press, New York, 1967).
[5] M. Kleman and O. Lavrentovich, *Soft Matter Physics* (Springer-Verlag, Berlin, 2003).
[6] J. Fukuda, Eur. Phys. J. B **1**, 173 (1998).
[7] G. Tóth, C. Denniston, and J. M. Yeomans, Phys. Rev. Lett. **88**, 105504 (2002).
[8] D. Svenšek and S. Žumer, Phys. Rev. E **66**, 021712 (2002).
[9] P. D. Olmsted and P. Goldbart, Phys. Rev. A **41**, R4578 (1990).
[10] T. Qian and P. Sheng, Phys. Rev. E **58**, 7475 (1998).
[11] A substrate usually defines an easy axis $\mathbf{n}_0$ for which the surface energy of the director $\mathbf{n}$ is minimal. Zenithal anchoring energy depends on out-of-plane rotations and azimuthal anchoring energy on in-plane rotations of $\mathbf{n}$.
[12] I. Dozov *et al.*, Appl. Phys. Lett. **77**, 4124 (2000).
[13] The electric field between two thin semi-infinite conductors located at $x < -D/2$ and $x > +D/2$ is $E(x) = 2V_a/[\pi D\sqrt{1-(2x/D)^2}]$. In the half center region $-D/4 < x < D/4$, it checks $E = 0.7(\pm 0.05)V_a/D$.
[14] A. Bogi, P. Martinot-Lagarde, I. Dozov, and M. Nobili, Phys. Rev. Lett. **89**, 225501 (2002).
[15] G. P. Chen, H. Takezoe, and A. Fukuda, Liq. Cryst. **5**, 341 (1989).
[16] M. L. Magnuson, B. M. Fung, and J. P. Bayle, Liq. Cryst. **19**, 823 (1995).
[17] B. R. Ratna and R. Shashidar, Mol. Cryst. Liq. Cryst. **42**, 113 (1977).
[18] This friction force is weak here, and we neglect it (in Fig. 3, $e_p \approx 2$ V/mm). It can be predominant for defect dynamics with other surface treatments. A study will be published elsewhere.
[19] Measurements of the dynamics of only $-1/2$ disclinations in 5CB were reported in P. E. Cladis *et al.*, Phys. Rev. Lett. **58**, 222 (1987) for a different experimental geometry. Using their published data, we obtain $\alpha_- = 658\ \mu\mathrm{m}^2/(\mathrm{V\,s})$ for an electric field range 10 times larger than ours at T_{eq}. Taking into account the logarithmic dependence in (3), this value is close to ours.
[20] We neglect here the rotational diffusion considered in G. Ryskin and M. Kremenetsky, Phys. Rev. Lett. **67**, 1574 (1991). Including this effect does not change significantly b.
[21] K. Skarp, S. Lagerwall, and B. Stebler, Mol. Cryst. Liq. Cryst. **60**, 215 (1980).
[22] H. J. Coles, Mol. Cryst. Liq. Cryst. **49**, 67 (1978).
[23] In order to check the influence of the elastic constant anisotropy $k = K_{33}/K_{11}$, we have compared free-pair (without external field) and π wall annihilations without flow. For the 5CB elastic constants, $r = 0.95$ (free-pair) and below numerical resolution of 1% (π wall). For a larger anisotropy $k = 2.5$: $r = 0.89$ (free-pair) compared to $r = 0.99$ (π wall).